Improper ferroelastic phase transition in a hydrogen-bonded metallocyanide-based (azetidinium)$_2$(H_3O)[$Co(CN)_6$] framework

Electronic Supplementary Information

by Marcin Moskwa*[a], Paweł Sobieszczyk[b], Julia W. Mikurenda[a], Piotr Zieliński[b], and Magdalena Rok*[a]

[a]*Faculty of Chemistry, University of Wroclaw, Joliot-Curie 14, 50-383 Wrocław, Poland.*

[b]*The H. Niewodniczański Institute of Nuclear Physics PAS, Radzikowskiego 152, 31-342 Kraków, Poland*

*Corresponding Author

E-mail address: marcin.moskwa@uwr.edu.pl (Marcin Moskwa), magdalena.rok@uwr.edu.pl (Magdalena Rok)

Table of Contents

Caption of Figs and Tables

S1. Sample preparation

Firstly, to obtain $H_3Co(CN)_6$, 3 g of $K_3Co(CN)_6$ was dissolved in about 20 ml of distilled water. Then the solution was filtered twice through an ion-exchange resin (Dowex) previously activated with 2M H_2SO_4. After that, obtained water solution of acid was placed on the heating plate and dried completely. In order to synthesise (azetidinium)$_2$(H_3O)[$Co(CN)_6$] (**1**), 1 g (10.69 mmol) of azetidine hydrochloride (Sigma Aldrich, purity: 97%) was mixed with 1.17g (5.36 mmol) of $H_3Co(CN)_6$ and dissolved in minimum amount of distilled water. Afterwards the solution was kept in desiccator over NaOH until crystals had started to form (see Fig. S1). The results of elemental analysis: C – 41.245%; N –31.94%; H – 5.611%; while theoretical content equals: C – 41.149%; N –32.991%; H – 5.467%. The homogeneity of $H_3Co(CN)_6$ and **1** were verified by PXRD (powder X-ray diffraction) (see Fig. S2). PXRD was performed on a D8 ADVANCE powder X-ray diffractometer with Cu radiation and a Vantec detector.

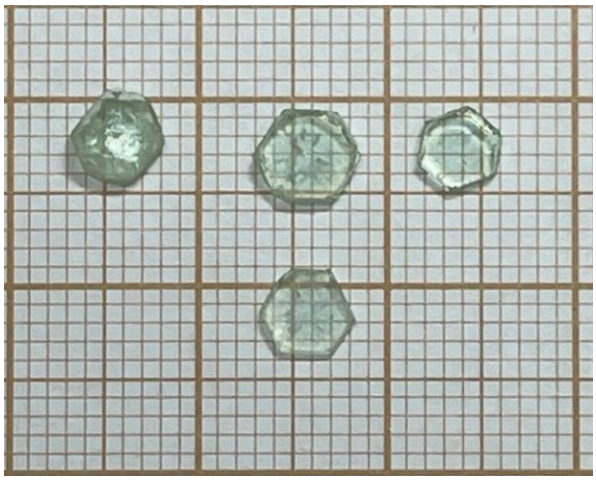

Fig. S1 The single-crystals of the **1** crystallized from the aqueous solution

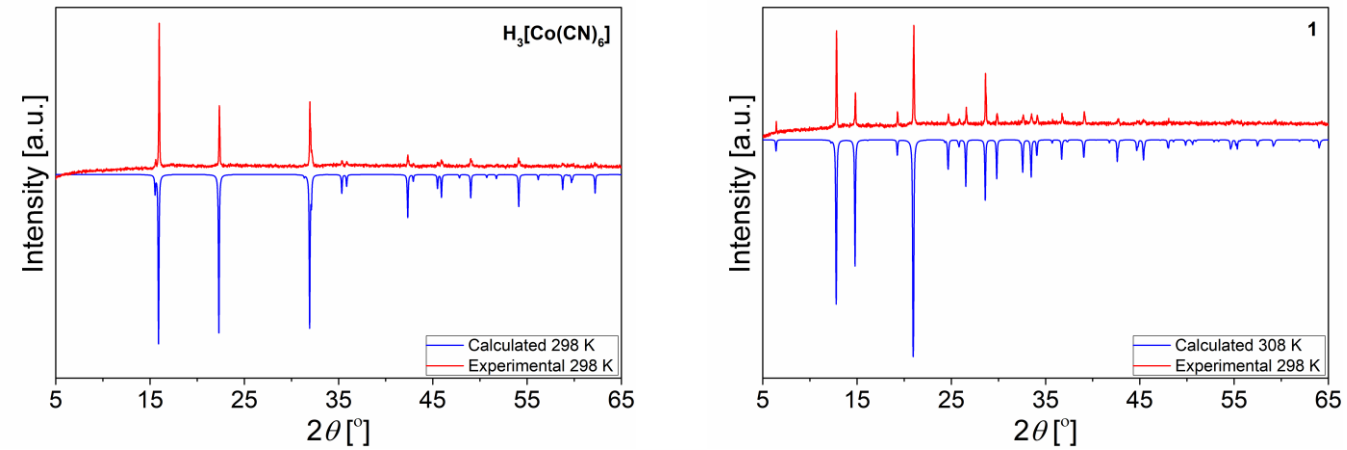

Fig. S2 Powder X-ray diffraction pattern for $H_3Co(CN)_6$ (ICSD No. 28502)[1] and **1** at room-temperature and calculated ones.

S2. Thermal Analysis

Differential scanning calorimetry (DSC**)** heating traces were obtained using a Mettler Toledo DSC 3 differential scanning calorimeter. The measurements were performed between 100 and 330 K. The enthalpies (ΔH) were calculated using the integral of DSC curves using the Mettler Toledo STARe Evaluation Software v.17.00. Based on the calculated enthalpy, the entropy was calculated using the equation $\Delta S = \frac{\Delta H}{T}$. Simultaneous thermogravimetric analysis (TGA) and differential thermal analysis (DTA) were carried out on a Setaram SETSYS 16/18 instruments in the temperature range 300-850 K with a ramp rate 5 $K \cdot min^{-1}$ in the nitrogen atmosphere (flow rate: 1 $dm^3 \cdot h^{-1}$), see Fig. S3.

Based on the Boltzmann equation, $\Delta S = R\ln(N)$, where R is the gas constant the value of *N* was calculated:

$$N = e^{\frac{\Delta S}{R}} = e^{\frac{15.4}{8.314}} = 6.37 \approx 6.4 \qquad \textbf{Eq. 1}$$

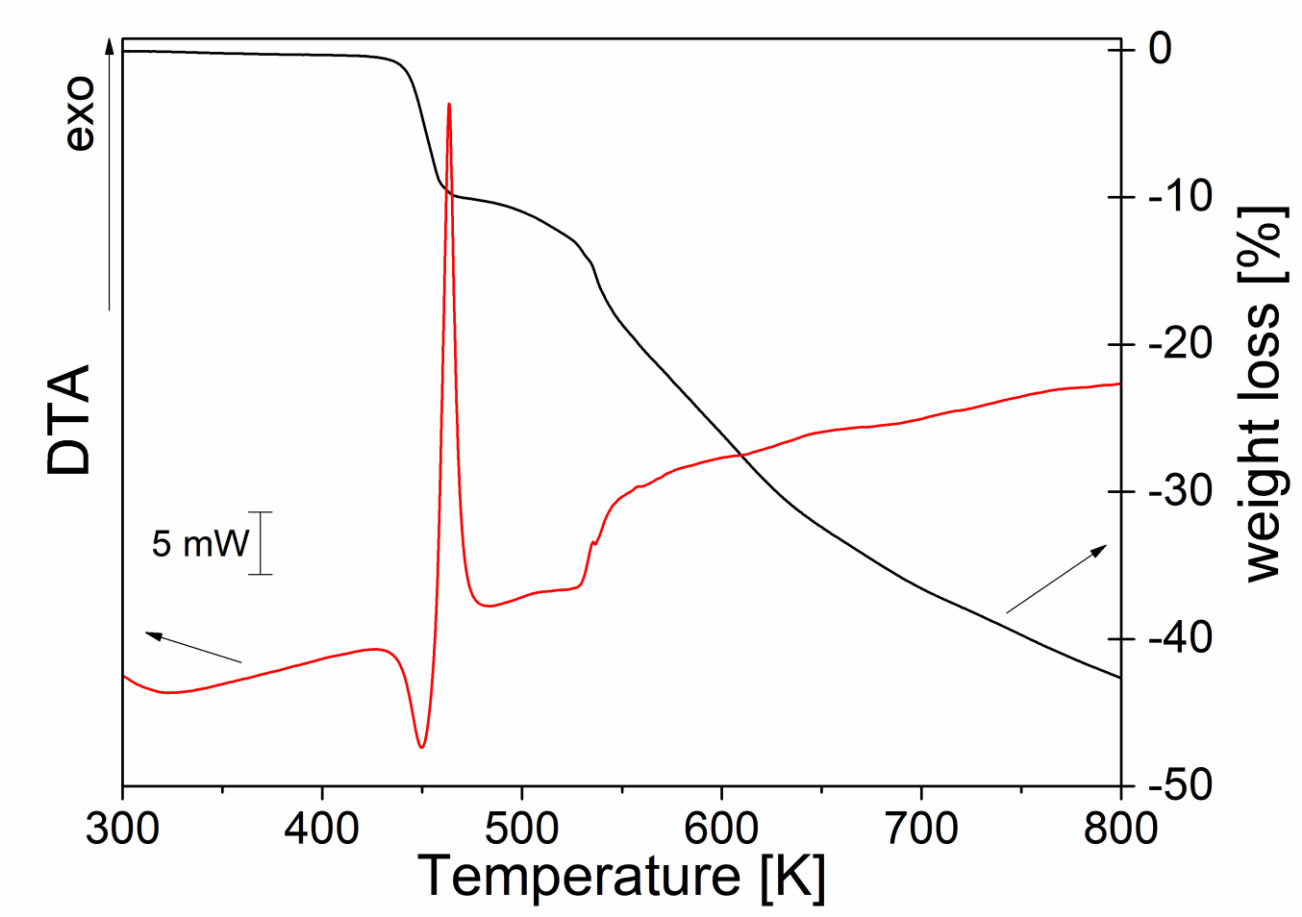

Fig. S3 TGA and DSC scans for **1** (sample mass m = 10.846 mg).

S3. Dielectric Properties

For dielectric measurements, single crystal samples were coated with silver conduction paste (Electron Microscopy Sciences, 503) on both sides as electrodes. The measurements were performed on crystallographically oriented monocrystal (S = 8mm^2, d = 1.2 mm) along c_{HT}-axis at frequencies range of 135Hz – 2MHz in the temperature range between 160 K and 300 K. The complex dielectric permittivity was measured using an Agilent E4980A Precision LCR The temperature was stabilized and controlled using an INSTEC STC200. The electric measurements were carried out in a controlled nitrogen atmosphere.

Fig. S4 presents the dielectric response that was measured on crystal **1** along to the $[001]_{HT}$ direction during the heating cycle. In addition to the characteristic anomaly at 297 K, we observe additional relaxation processes in both the HT and LT phases.

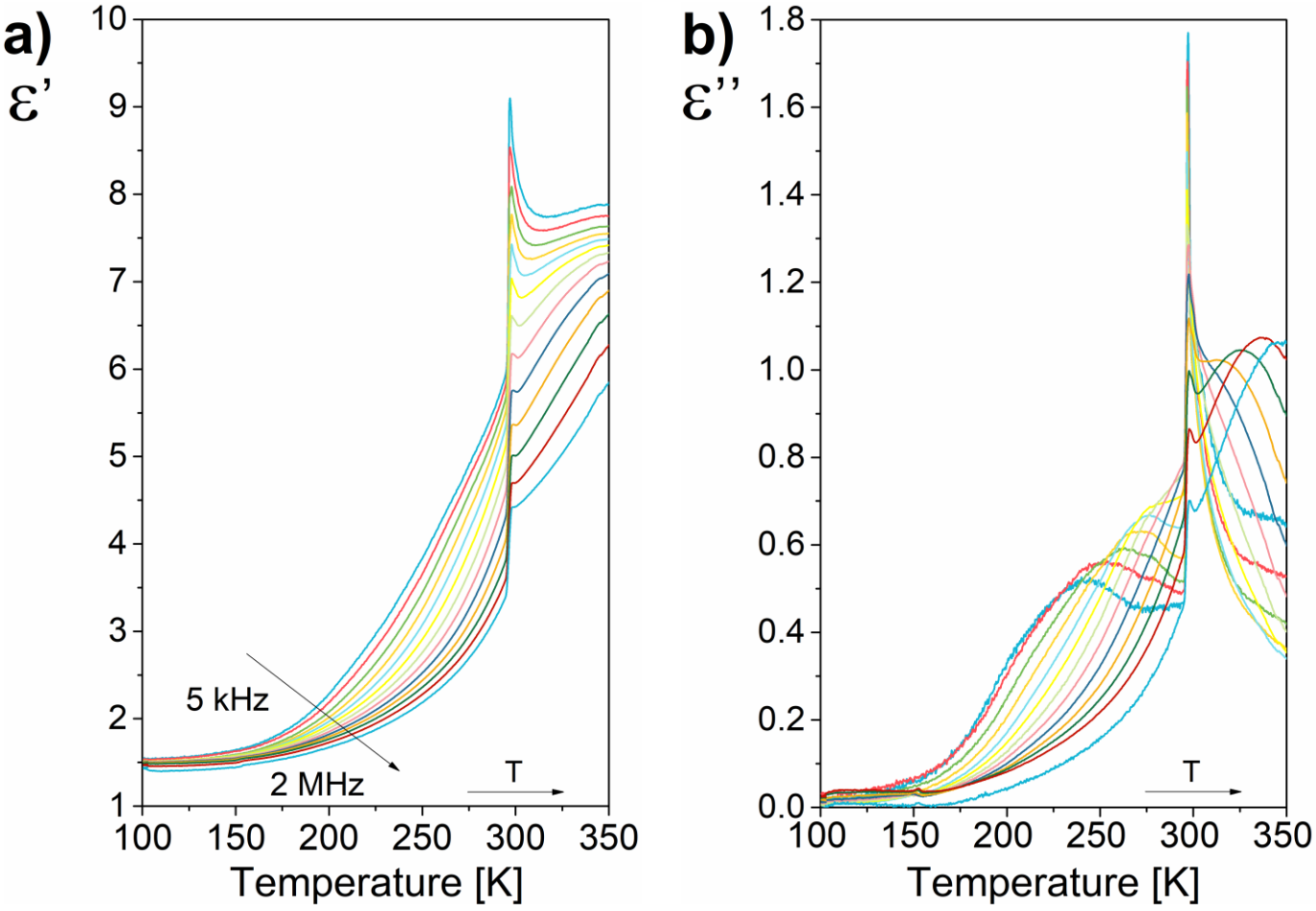

Fig. S4 The temperature dependence of the dielectric permittivity, a) ε' and b) ε'', obtained on heating run for single crystals perpendicular to the [001].

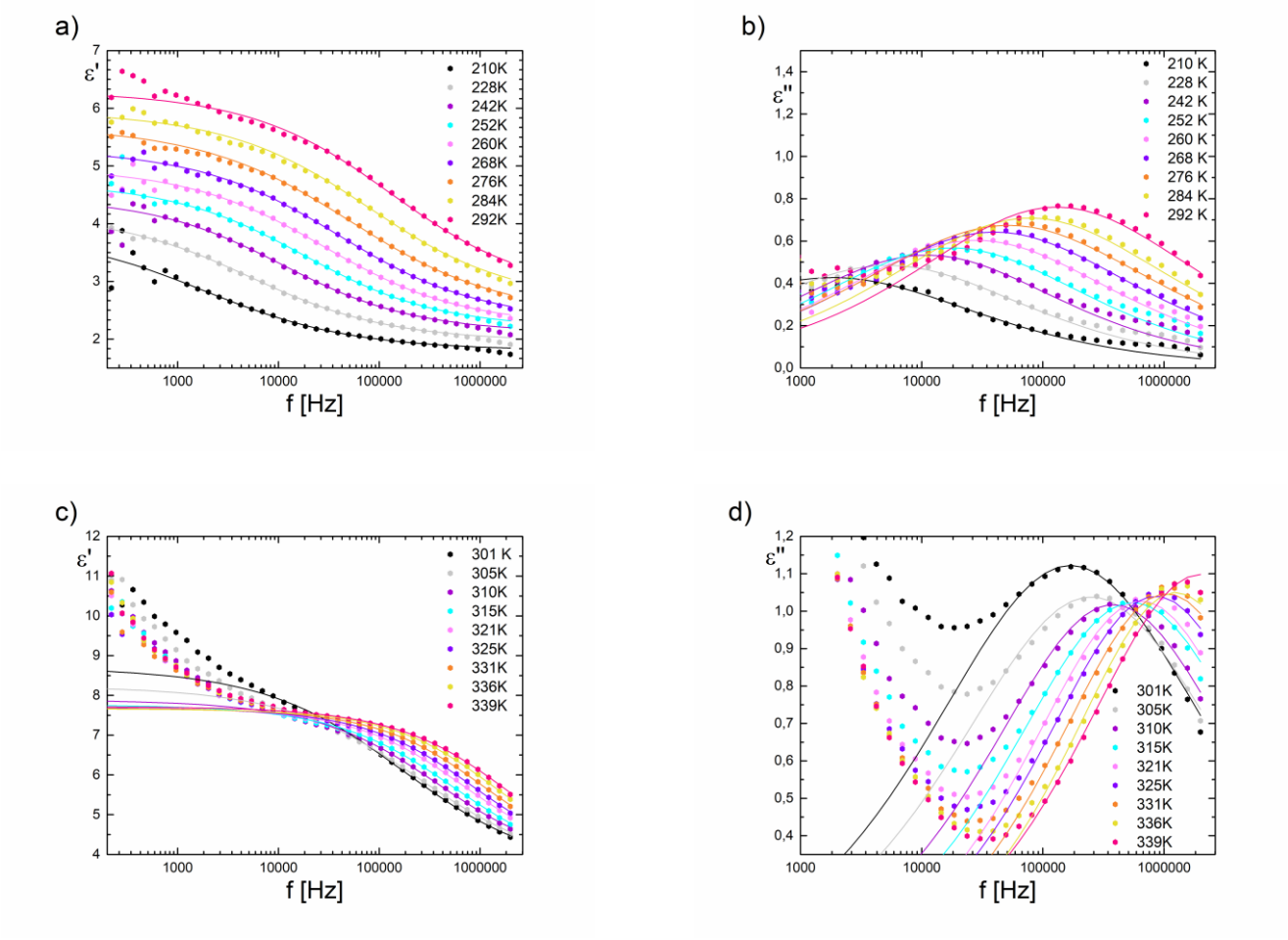

Fig. S5 The frequency dependence of the dielectric permittivity, ε' and ε", obtained on heating run for single-crystals along the c_{HT}-axis. Data was presented for chosen temperatures from (a, b) **LT** and (c, d) **HT** phase.

Our analysis proves that the dielectric absorption can be described by a one-parametric dielectric response function of the Cole–Cole[2] in the whole temperature range (Fig. S5).

$$\frac{\varepsilon' - \varepsilon_\infty}{\varepsilon_s - \varepsilon_\infty} = \frac{1 + \left(\frac{f}{f_c}\right)^{(1-\alpha)} \sin\left(\frac{a\pi}{2}\right)}{1 + \left(\frac{f}{f_c}\right)^{2(1-\alpha)} + 2\left(\frac{f}{f_c}\right)^{(1-\alpha)} \sin\left(\frac{a\pi}{2}\right)}$$

$$\frac{\varepsilon''}{\varepsilon_s - \varepsilon_\infty} = \frac{1 + \left(\frac{f}{f_c}\right)^{(1-\alpha)} \cos\left(\frac{a\pi}{2}\right)}{1 + \left(\frac{f}{f_c}\right)^{2(1-\alpha)} + 2\left(\frac{f}{f_c}\right)^{(1-\alpha)} \sin\left(\frac{a\pi}{2}\right)}$$

Eq. 2

Where ε_s and ε_∞ are the static and optical permittivity, respectively, and f_c is the frequency of the relaxation process. The average values of relaxation times $\tau = \frac{1}{(2\pi f_c)}$ were obtained from fitting the Cole-Cole Eq. in the range of frequencies from 135 Hz to 2 MHz. A theoretical model was fitted to the experimental points for selected temperatures for both HT and LT phases. The parameters obtained from this fitting are shown in **Table S1**. The parameter α appearing in the Cole-Cole Eq. 2 describes the relaxation time distribution. The α values close to zero suggest that the distributions of the relaxation are very narrow, and the observed dielectric relaxation processes are monodispersive. In case **1**, both in the HT and LT phases, the parameters presented in **Table S1** vary between 0.35 and 0.56, which indicates that in those temperature regions, we deal with a polydispersive relaxation process. In the case of the HT phase, the absorption maxima just after PT move toward frequencies above 1 MHz into the microwave range. The conclusion is that in this phase we have a free and quite fast movement, which may resemble the overall molecular tumbling which occurs in plastic phase. Based on the Arrhenius relation (τ), the activation energy E_a was estimated to be constant at *ca*. 28 and 50 kJ/mol for LT and HT phases, respectively (see Fig. S6).

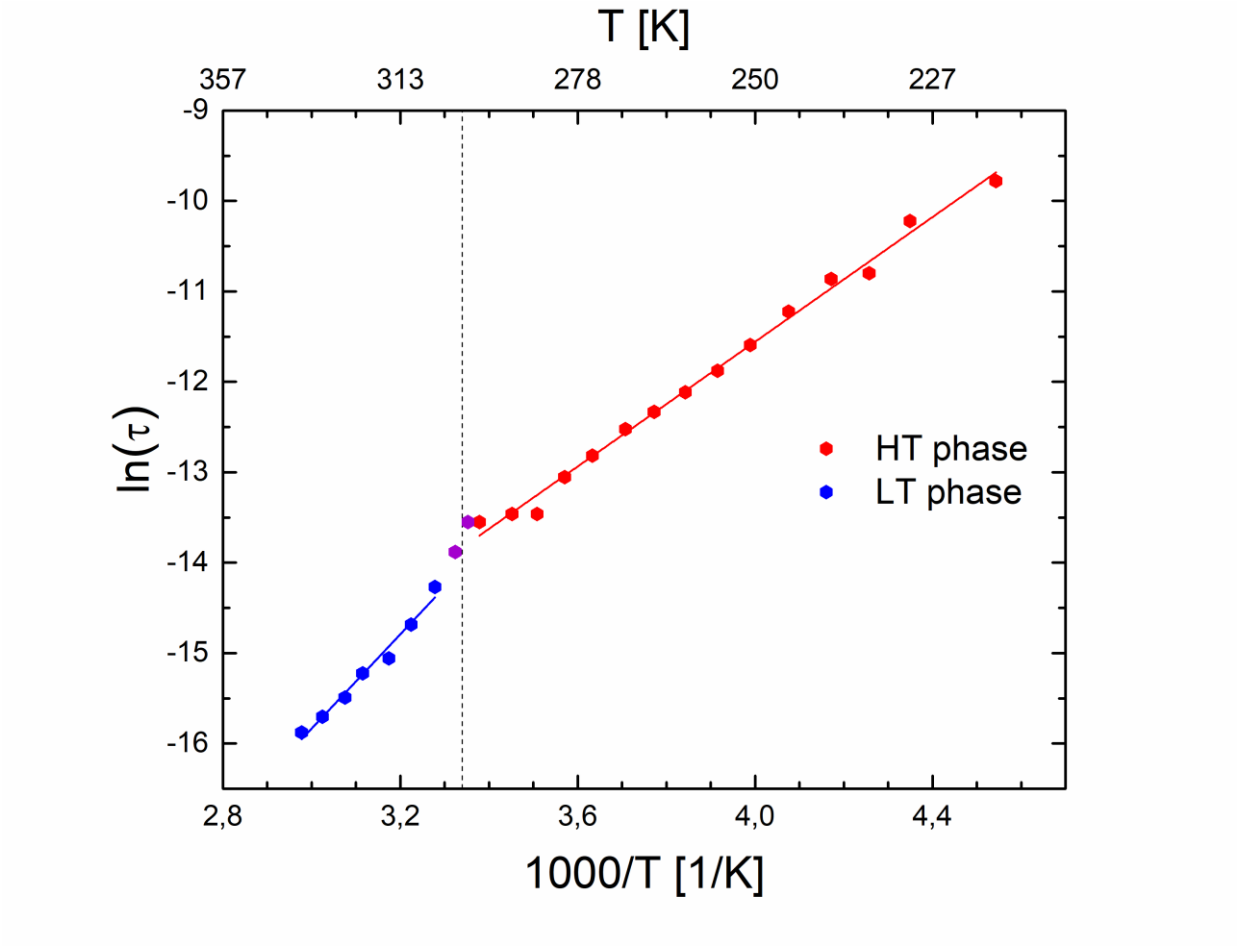

Fig. S6 Arrhenius plot of relaxation time in HT as well LT phases.

Table S1. Temperature dependence of the dielectric parameters: relaxation time (τ), distribution parameter (α), and dielectric increment ($\varepsilon_0 - \varepsilon_\infty$) for **1**.

LT phase								
T [K]	220	235	245	255	265	275	285	296
τ [μs]	56.7	20.4	13.4	6.95	4.40	2.72	1.42	1.31
α	0.56	0.50	0.52	0.49	0.51	0.50	0.46	0.45
ε_0	4.3	4.4	4.7	4.9	5.2	5.6	5.8	7.8
ε_∞	1.8	1.9	2.0	2.1	2.2	2.3	2.6	3.1
HT phase								
T [K]	305	310	315	321	325	331	336	339
τ [μs]	0.637	0.419	0.289	0.245	0.187	0.152	0.127	0.0796
α	0.47	0.43	0.42	0.38	0.39	0.37	0.35	0.40
ε_0	8.2	7.9	7.8	7.7	7.7	7.7	7.7	7.7
ε_∞	3.6	3.7	3.6	3.8	3.7	3.8	3.9	3.4

S4. Crystal structure determination

The single-crystal X-ray diffraction (SCXRD) data for **1** was performed on a Agilent Technologies Xcalibur, Gemini-ultra *κ*-axis four-circle diffractometers equipped with an Oxford Cryosystem cooler using graphite monochromated MoKα radiation with graphite-monochromated Mo-Kα radiation (0.71073 Å). The data were collected at 308, and 200 K. Data reduction and analysis were carried out with the CrysAlis Pro program.[3] The crystal structures were solved by direct methods using the *SHELXS*-2014/7 program and refined by the full-matrix least-squares using all F^2 data, as implemented by the *SHELXL*-2014/7 program.[4,5] Hydrogen atoms were located according to the respective molecules or were found in $\Delta\rho$ maps. The atomic displacement factors of disordered atoms were refined with DFIX, EADP and ISOR limitations. The low-temperatures diffraction data of **1** reveal extensive twinning of the crystal. The result is the domain structure that appears on the phase transition from trigonal (high-temperature, HT) to monoclinic (low-temperature, LT) phase. Diffraction data for the phase **1-LT** was reduced as two-component twins and refined with the use of the HKLF 5 type reflection file (a 0.566(2):0.434(2) ratio). The crystal data together with the experimental and refinement details are given in Table S1. Crystallographic data for the structures reported in this paper have been deposited with the CCDC No. **2247736** and **2247737**.

Table S2. Crystal data, experimental details, and structure refinement results for **1** at 308 and 200 K.

	1-HT	**1-LT**
Chemical formula	$2(C_3H_8N^+)\cdot H_3O^+\cdot C_6CoN_6^{3-}$	
M_r	350.28	
Crystal system, space group	Trigonal, $R\bar{3}m$:*H*	Monoclinic, $P2_1/a$*
Temperature (K)	308(2)	200(2)
a, *b*, *c* (Å)	8.4901(3), 8.4901(3), 41.463(2)	14.497(3), 8.5378(3), 14.317(2)
β (°)		108.12(3)
V (Å^3)	2588(2)	1684(3)
Z	6	4
Radiation type	Mo *K*α	Mo *K*α
μ (mm^{-1})	1.01	1.03
Crystal size (mm)	0.18 × 0.16 × 0.14	0.18 × 0.16 × 0.14
Diffractometer	Xcalibur, Ruby, Gemini ultra	Xcalibur, Ruby, Gemini ultra
No. of measured, independent and observed [$I > 2\sigma(I)$] reflections	4115, 790, 659	7535, 7535, 3779
R_{int}	0.020	Dataset merged
$(\sin\theta/\lambda)_{max}$ (Å^{-1})	0.650	0.679
$R[F^2 > 2\sigma(F^2)]$, $wR(F^2)$, *S*	0.040, 0.108, 1.07	0.037, 0.095, 1.07
No. of reflections	790	7535
No. of parameters	74	203
No. of restraints	42	0
$\Delta\rho_{max}$, $\Delta\rho_{min}$ (e Å^{-3})	0.46, -0.36	0.57, -0.30

* - nonstandard setting of space group $P2_1/c$ (no. 14)

Table S3. Hydrogen-bond geometry [Å, º] for **1** at a) 308 K (HT) and b) 200 K (LT).

a)

D—H···*A*	H···*A*	*D*···*A*	*D*—H···*A*
O1*H*—H1*H*···N2^{i}	1.76	2.606(3)	178
N1*A*—H1*A*···N1^{ii}	2.09	2.965(5)	168

Symmetry codes: (i) -*y*+1, *x*-*y*+1, *z*; (ii) -*y*+1, *x*-*y*, *z*.

b)

D—H···*A*	H···*A*	*D*···*A*	*D*—H···*A*
N1*A*—H1*A*2···N1	1.98	2.861(4)	161
N1*A*—H1*A*1···N2^{i}	2.04	2.922(4)	163
N1*B*—H1*B*2···N2^{ii}	2.32	3.169(5)	156
N1*B*—H1*B*1···N3^{iii}	2.02	2.902(4)	164
O1*H*—H3*H*···N4	1.77	2.619(4)	176
O1*H*—H2*H*···N5^{iv}	1.81	2.630(4)	163
O1*H*—H1*H*···N6^{v}	1.74	2.581(4)	169

Symmetry codes: (i) *x*+1/2, -*y*+3/2, *z*; (ii) -*x*+1, -*y*+1, -*z*+2; (iii) *x*+1/2, -*y*+1/2, *z*; (iv) -*x*+1/2, *y*+1/2, -*z*+1; (v) -*x*+1/2, *y*-1/2, -*z*+1.

Table S4. Comparison of the fractional atomic coordinates for **1** at 308 K and 200 K.

308 K	*x*	*y*	*z*	**200 K**	*x*	*y*	*z*
Co1	0.3333	0.6667	0.6667	Co1	0.5000	0.5000	1.0000
Co2	0.0000	1.0000	0.5000	Co2	0.0000	0.5000	0.5000
C1	0.4393(3)	0.5607(3)	0.64078(9)	C1	0.5772(3)	0.4754(4)	0.9150(2)
N1	0.5050(3)	0.4950(3)	0.62631(11)	N1	0.6285(2)	0.4602(4)	0.86802(19)
				C2	0.4134(3)	0.6390(4)	0.9099(2)
				N2	0.3589(2)	0.7245(4)	0.85999(19)
				C3	0.4216(3)	0.3248(4)	0.9425(2)
				N3	0.3730(3)	0.2179(4)	0.91312(19)
C2	0.1054(2)	0.8946(2)	0.52618(8)	C4	0.1274(3)	0.4941(4)	0.5897(2)
N2	0.1691(2)	0.8309(2)	0.54164(8)	N4	0.2050(2)	0.4915(4)	0.64305(19)
				C5	0.0394(3)	0.3653(4)	0.4141(2)
				N5	0.0626(2)	0.2803(4)	0.3632(2)
				C6	0.0325(3)	0.6791(4)	0.4387(2)
				N6	0.0516(2)	0.7883(4)	0.4018(2)
O1H	0.3333	0.6667	0.56527(8)	O1H	0.39476(18)	0.5055(3)	0.69559(13)
N1A	0.6667	0.3333	0.58361(11)	N1A	0.7455(2)	0.5199(3)	0.74361(18)
C2A	0.5128(5)	0.2564(3)	0.55906(13)	C2A	0.6762(3)	0.5755(6)	0.6473(2)
C21A	0.5898(3)	0.4102(3)	0.55910(13)				
C3A	0.6667	0.3333	0.53450(19)	C3A	0.7112(3)	0.4517(5)	0.5932(2)
				C4A	0.7832(3)	0.3975(5)	0.6902(2)
N1B	0.691(2)	0.432(2)	0.6872(3)	N1B	0.8129(2)	0.4133(4)	1.07203(19)
C2B	0.536(2)	0.240(2)	0.6936(4)	C2B	0.8403(3)	0.5826(5)	1.0818(3)
C3B	0.7748(13)	0.4288(17)	0.7195(2)	C3B	0.9331(4)	0.5399(5)	1.1637(3)
				C4B	0.8948(3)	0.3771(5)	1.1637(2)

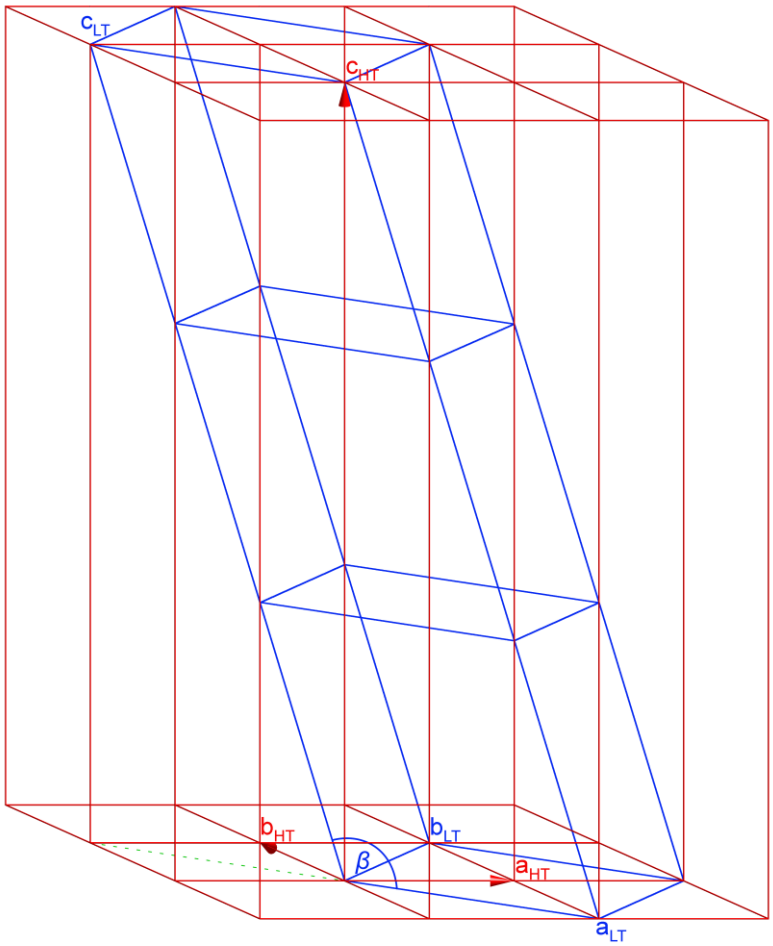

Fig. S7 Relation of the trigonal (**1-HT** red line) and monoclinic (**1-LT** blue line) unit cells in **1**.

Table S5. The geometric and calculated relationship of the unit cells of **1**.

$R\bar{3}m$ **(166) – HT**	$P2_1/a$*** (14, *nonstandard) – LT**	**Calculated**
$a_{HT} = 8.4901$ Å	$a_{LT} = 14.497$ Å	$a_{LT} = 2a_{HT}\cos\frac{60°}{2} = 14.705$ Å
	$b_{LT} = 8.5378$ Å	$b_{LT} = a_{HT} = 8.4901$ Å
$c_{HT} = 41.463$ Å	$c_{LT} = 14.317$ Å	$c_{LT} = \frac{1}{3}((a_{LT})^2 + (c_{HT})^2)^{\frac{1}{2}} = 14.641$ Å
	$\beta = 108.12°$	$\beta = 180° - \tan^{-1}\left(\frac{c_{HT}}{a_{LT}}\right) = 109.27°$

S5. Group theoretical description of the symmetry changes in the phase transition

The full symmetry reduction $R\bar{3}m \rightarrow P2_1/c$ ($P2_1/a$) involves, however, doubling of the unit cell *i.e.* a reduction of translational symmetry. Therefore, the phase transition is an antiferrodistorive improper ferroelastic.([6] p. 440) The primary order parameter is any quantity that transforms according to an irreducible representation of the group $R\bar{3}m$ with a wave vector at the border of the 1st Brillouin zone. When reported to the reference system ($a_{HT,}$ b_{HT}, c_{HT}) of Figure S7 of ESI the wave vector has the components $\left(\frac{\pi}{a_{HT,}}, \frac{\pi}{a_{HT,}}, 0\right)$. The wave vector is denoted by FA.[7] The wave vector group (little group) of this wave vector involves the 2/*m* point factor group composed with all the translations of the group $R\bar{3}m$. The group $R\bar{3}m$ being symmorphic the projective (loaded) representations are identical with the ordinary representations of the point group 2/*m*.[7–9] One should remark that the space group $P2_1/c$ of the LT phase is a subgroup of the above mentioned little group. Moreover, the point factor groups of both space groups are identical, *i.e.* the space group $P2_1/c$ is a subgroup of the little group with only translational symmetry broken. The point symmetry operations are the same. But the double axis and the mirror plane in $P2_1/c$ are composed with a non-lattice translation. Therefore, the active representation driving this phase transition is such that the double axis and the mirror plane correspond to -1, which when composed with the lost translation, also corresponding to -1 due to the wave vector, produce a unity 1. This representation is B_g, (irreducible representations of the point group 2/*m*) which has to be used as the loaded representation of the point group 2/*m* in the construction of the irreducible representation of the space group $R\bar{3}m$ driving the symmetry reduction $R\bar{3}m \rightarrow P2_1/c$ [see [10], point 5]. A soft mode or a central peak (in the case of and OD transition) is, therefore, expected at the wave vector FA on the B.z. border (Brillouin zone border) with the loaded (projective) representation B_g. The 6-fold symmetry reduction corresponds to the 6-fold reduction of the orientational AZE^+ cations. There are also six domains of the monoclinic phase. The domains related by rotations by $2\pi/3$ and $4\pi/3$ are ferrelastic domains. Every ferroelastic domain has two antiphase variants shifted with respect to each other by a vector (½, ½, 0) in the conventional setting of the space group $P2_1/c$.

S6. Optical measurements

The optical microscopy observation was carried out using an Olympus BX53 microscope combined with a LINKAM THM-600 heating/cooling stage, where the temperature was stabilized to within 0.1 K.

References

1 L. Pauling and P. Pauling, *Proc. Natl. Acad. Sci.*, 1968, **60**, 362–367.
2 K. S. Cole and R. H. Cole, *J. Chem. Phys.*, 1941, **9**, 341–351.
3 CrysAlisPro 1.171.41.80a (Rigaku OD, 2020).
4 G. M. Sheldrick, *Acta Crystallogr. A*, 2008, **64**, 112–122.
5 G. M. Sheldrick, *Acta Crystallogr.*, 2015, **C71**, 3–8.
6 V. Wadhawan, *Introduction to Ferroic Materials*, CRC Press, London, 2014.
7 M. I. Aroyo, A. Kirov, C. Capillas, J. M. Perez-Mato and H. Wondratschek, *Acta Crystallogr. Sect. A*, 2006, **62**, 115–128.
8 C. J. Bradley and A. P. Cracknell, *The mathematical theory of symmetry in solids: representation theory for point groups and space groups*, Clarendon Press, Oxford : New York, 2010.
9 G. Ya. Lyubarskii, *The Application of Group Theory in Physics*, Pergamon, Pergamon, 1st Edition., 1960.
10 P. W. Atkins, M. S. Child and C. S. G. Phillips, *Tables for Group Theory*, Oxford University Press, 2008.